Transcriptome profiling in swine macrophages infected with African swine fever virus at single-cell resolution

Yuxuan Zheng[a,1], Su Li[b,1], Shi-Hua Li[a,1], Shaoxiong Yu[b,1] (iD), Qihui Wang[a,c] (iD), Kehui Zhang[b], Liang Qu[b], Yuan Sun[b], Yuhai Bi[a,c,2], Fuchou Tang[d,e,f,2], Hua-Ji Qiu[b,2] (iD), and George F. Gao[a,c,2] (iD)

African swine fever virus (ASFV) is the causative agent of African swine fever, a highly contagious and usually fatal disease in pigs. The pathogenesis of ASFV infection has not been clearly elucidated. Here, we used single-cell RNA-sequencing technology to survey the transcriptomic landscape of ASFV-infected primary porcine alveolar macrophages. The temporal dynamic analysis of viral genes revealed increased expression of viral transmembrane genes. Molecular characteristics in the ASFV-exposed cells exhibited the activation of antiviral signaling pathways with increased expression levels of interferon-stimulated genes and inflammatory- and cytokine-related genes. By comparing infected cells with unexposed cells, we showed that the unfolded protein response (UPR) pathway was activated in low viral load cells, while the expression level of UPR-related genes in high viral load cells was less than that in unexposed cells. Cells infected with various viral loads showed signature transcriptomic changes at the median progression of infection. Within the infected cells, differential expression analysis and coregulated virus–host analysis both demonstrated that ASFV promoted metabolic pathways but inhibited interferon and UPR signaling, implying the regulation pathway of viral replication in host cells. Furthermore, our results revealed that the cell apoptosis pathway was activated upon ASFV infection. Mechanistically, the production of tumor necrosis factor alpha (TNF-α) induced by ASFV infection is necessary for cell apoptosis, highlighting the importance of TNF-α in ASFV pathogenesis. Collectively, the data provide insights into the comprehensive host responses and complex virus–host interactions during ASFV infection, which may instruct future research on antiviral strategies.

African swine fever virus | single-cell RNA sequencing | macrophage | virus–host interaction | tumor necrosis factor alpha

African swine fever (ASF), caused by African swine fever virus (ASFV), is a severe and highly contagious disease in domestic pigs and wild boars that is listed by the World Organisation for Animal Health. The disease was first identified in Kenya in 1921, and is currently distributed in many sub-Saharan African countries, the Russian Federation, Trans-Caucasus, some Eastern and Central European countries, Sardinia, and Southeastern and Eastern Asia. ASF has severely affected the global pig industry (1).

ASFV belongs to the family *Asfarviridae* and is a large, enveloped, double-stranded DNA virus with an average diameter of about 250 nm. Mature ASFV virions consist of an outer membrane, capsid, inner membrane, core shell, and viral genome. The genome size of different ASFV strains ranges from 170 to 194 kb and encodes 151 to 174 open reading frames (2, 3). The functions of more than half of the viral genes remain unknown (4).

ASFV mainly infects and replicates in swine macrophages (5). Viral replication relies on a highly coordinated process consisting of temporally and spatially controlled expression of different viral genes, and is involved in the complex and multifaceted interplay between host cellular pathways. ASFV infection induces cell apoptosis in macrophages. The abilities to cause macrophage death are the main factors used to evaluate the virulence of ASFV (6). However, the molecular mechanisms underlying ASFV pathogenesis remain largely unknown.

High-throughput single-cell RNA-sequencing (scRNA-seq) analysis provides a powerful and unbiased strategy for the characterization of individual cells infected with viruses, which can be masked at the population level (7–9). Various cell types can be identified using scRNA-seq and the expression profiles of each individual cell can be explored. Based on viral loads within cells, scRNA-seq can reveal transcriptomic changes between infected and uninfected cells, providing a further view of host cellular response mechanisms to viruses.

Here, we systematically profiled the transcriptomes of ~108,000 individual cells using the high-throughput scRNA-seq method of 10× Genomics. The cells were

Significance

African swine fever virus (ASFV) causes a severe and highly contagious disease in pigs and wild boars, but no commercial vaccines or antivirals are available currently. Understanding the mutual antagonism between virus and host factors during ASFV infection may facilitate the development of new vaccines and antivirals. Our work profiled transcriptomes of swine macrophages infected with ASFV through single-cell RNA-sequencing technology. Identified dynamic transcriptome events of viral genes provide molecular characteristics of ASFV during infection. Moreover, virus–host interactions imply the regulation pathway of viral replication in host cells, which may guide research on antiviral strategies and dissection of ASFV pathogenesis.

Fig. 1. Distinct cell types revealed by scRNA-seq in alveolar lavage fluid. (*A* and *B*) Identification of ASFV infection. Immunofluorescence analysis of ASFV viral protein p72 in cells infected with ASFV (*A*), and viral titers in the supernatants examined by hemadsorption assay HAD_{50} (*B*). Data are shown as mean value ± SD. (Scale bars, 200 μm.) (*C*) Schema of this study design. (*D*) UMAP plot showing cell types in unexposed and exposed cells. (*E*) UMAP plots showing the group information of cells. (*F*) Dot plot showing scaled expression levels of cell type–specific genes in unexposed and exposed cells. Expression levels in each gene are scaled, ranging from 0 to 1. The dot color and size indicate expression levels and the percentage of expressed cells, respectively. DC, dendritic cell; Mac., macrophage; Mast, mast cell; Pro., proliferative cell; T, T cell.

collected from 13 samples containing primary porcine alveolar macrophages (PAMs) in vitro at times corresponding to the baseline, six time points during ASFV infection, and six time points paired with PAM controls to compare the transcriptomes. The scRNA-seq analysis enabled the distinction of macrophages infected with various viral loads, permitting a comprehensive analysis of host and viral gene expression profiles following ASFV infection. More specifically, we demonstrated that tumor necrosis factor alpha (TNF-α) is required for cell apoptosis induced by ASFV infection in PAMs.

Results

Single-Cell Transcriptome Landscape in ASFV-Infected PAMs.
To understand both host and viral dynamic changes of transcriptional states in PAMs after ASFV infection, we collected phosphate-buffered saline–treated PAMs as the control and PAMs infected with ASFV at different time points. To verify the susceptibility of ASFV in PAMs, the cells were infected with ASFV at a multiplicity of infection (MOI) of 1. The intensity of p72 (coded by viral gene *B646L*) could be detected in the ASFV-infected group by indirect immunofluorescence assay, and viral titers in the supernatants were increased during infection (Fig. 1 *A* and *B*). Then, PAMs collected at all time points in the ASFV-infected and uninfected groups were used

for scRNA-seq with 10× Genomics (Fig. 1*C*). After stringent cell filtration, 62,398 and 46,090 high-quality single cells from the uninfected group and ASFV-infected group were obtained for subsequent analyses, respectively (*SI Appendix*, Fig. S1 *A and B*). An average of 20,748 unique molecular identifiers (UMIs) and 3,228 genes from the host and virus was detected (*SI Appendix*, Fig. S1*B*). To simplify the explanation, cells in the uninfected or ASFV-infected groups are called unexposed cells or exposed cells hereafter, respectively. In addition, exposed cells were further separated into bystander cells and infected cells. We investigated the distribution of viral loads and the number of genes in exposed cells (*SI Appendix*, Fig. S1*C*). There were two observed clusters with low and high viral loads at 2, 6, 10, and 15 h postinfection (hpi). Only one cluster with low viral loads was observed at 24 and 36 hpi, which suggested that the number of cells with high viral loads decreased during infection.

To exclude the potential transcriptome bias of exposed cells, we first analyzed unexposed cells for identifying cell types. Unsupervised clustering analysis and uniform manifold approximation and projection (UMAP) nonlinear dimensionality reduction analyses combined with gene expression profiles of well-known marker genes identified five main immune cell types (*SI Appendix*, Fig. S1 *D–F* and Dataset S1). Supervised clustering analysis was then performed, and the clustering

information and transcriptomic patterns revealed within unexposed cells were projected onto exposed cells (Fig. 1*D*, *SI Appendix*, Fig. S1 *G* and *H*, and Dataset S1). Consistent with a previous report (10), macrophages were the main cell type in alveolar lavage fluid in the uninfected (97.8% of the cells) and ASFV-infected groups (96.9%). Unexposed cells were separated from exposed cells in the UMAP plot, suggesting that ASFV infection and exposure induced global transcriptomic changes in the host (Fig. 1*E*). We also performed principal component analysis (PCA) with all cells, and observed the transcriptomic difference between unexposed cells and exposed cells (*SI Appendix*, Fig. S1*I*). The identification of differentially expressed genes (DEGs) among various cell types revealed unique cell type–specific signatures (Fig. 1*F*). Similar expression patterns were detected between unexposed and exposed cells, indicating that ASFV infection had a minimal effect on the identity of immune cells (Fig. 1*F*).

Varied Infection Rates of Macrophages at Various Time Points. Determinations of the ASFV transcript and viral load revealed variations in viral entry in different cells (Fig. 2*A* and *SI Appendix*, Fig. S2 *A* and *B*). In our scRNA-seq data of all exposed cells, we detected 95.5% (170 of 178) expressed ASFV genes within 36 hpi, and unexpressed genes might be pseudogenes or transcripts that are generated in later infection stages. Since macrophages are the main target cells of ASFV infection, our study focused on macrophages in the subsequent analyses (11, 12). For macrophages, ASFV transcripts rapidly increased at initial infection stages from 2 to 6 hpi, and then decreased from 10 hpi to later stages (Fig. 2*B* and *SI Appendix*, Fig. S2*C*). This showed that a balance between the host immune process and viral invasion process might exist at 6 and 10 hpi.

According to a statistical model considering ambient RNA contamination (7), the viral load was used to infer infected and bystander macrophages among exposed cells. The maximum percentage of infected macrophages was 47.8% at 6 hpi, with subsequent decreases with time to a minimum value of 5.8% at 24 hpi (Fig. 2*C* and Dataset S1). The messenger RNA (mRNA) copies of various ASFV genes in macrophages were then investigated, and viral 5′ and 3′ transcripts were captured in infected macrophages. *MGF_110-7L*, *MGF_110-3L*, *MGF_110-5L-6L*, and *CP204L* constitute a high percentage of mRNA copies in the ASFV genome (Fig. 2*D*). In contrast, hardly any viral transcripts were detected in bystander macrophages. Early-transcription ASFV genes (for example, *K205R* and *X69R*) were highly expressed in early stages after infection, and late-transcription ASFV genes (for example, *I196L*, *K421R*, and *B646L*) were highly expressed in later stages, indicating active viral transcription at corresponding time points (Fig. 2*E*). Notably, the kinetics of *B646L* transcription in scRNA-seq data is consistent with the result obtained from quantitative real-time RT-PCR (qRT-PCR) (Fig. 2 *E* and *F*). Above all, these results suggest that the scRNA-seq data provided reliable expression patterns of ASFV genes in host cells. The generated gene annotation was valuable concerning the description, location, and function of viral genes (Dataset S2).

Dynamic Expression Changes of Viral Genes during Infection. Next, we explored the top-ranked viral genes based on expression levels in infected cells. The *MGF_110-7L*, *MGF_110-5L-6L*, *MGF_110-3L*, and *MGF_110-4L* genes were the top-ranked viral genes at any time point during infection, and these genes were associated with endoplasmic reticulum (ER) functions (Fig. 2*G*, *SI Appendix*, Figs. S2*D* and S3, and Dataset S2). In addition,

these four genes belong to the ASFV MGF (multigene) family, which can be mainly divided into MGF_100, MGF_110, MGF_300, MGF_360, and MGF_505/530 based on genome locations. The scRNA-seq data were further confirmed by qRT-PCR for detection of mRNA transcription of *MGF_110-7L*, *MGF_110-5-6L*, and *MGF_110-3L* genes (Fig. 2*F*). Genes in variable regions on both termini of the genome are not essential for virus proliferation in vitro, but most are involved in inhibiting the production of type I interferons (IFNs) in the host and regulating the expression of proinflammatory cytokines. Then, genes involved in the antagonism of the IFN pathway, which included *MGF_360-15R*, *MGF_505-3R*, and *MGF_505-4R*, also generated markedly more mRNA copies than those of other viral genes, suggesting that the expression of viral genes triggered IFN inhibition at early stages of infection and thus facilitated viral growth in host cells by prolonging the survival time of the infected cells (Fig. 2*G*) (13, 14).

We also noticed that the *A224L* gene was expressed in most of the infected cells (Fig. 2*G*). As a member of the family of apoptosis inhibitor proteins, the *A224L* gene inhibits caspase 3 activation and protects cells from apoptosis (15). To prevent programmed cell death and ensure virus replication, the virus can encode several genes that block the apoptosis process. In addition, the ASFV *A179L* gene, a homolog of the antiapoptotic Bcl-2 protein, prolongs host cell survival during viral genomic replication (16, 17). Our scRNA-seq analysis demonstrated that *A179L* was expressed at both middle and late stages of infection, indicating that it plays a crucial role in cell survival at various stages of the virus life cycle (*SI Appendix*, Fig. S2*D*).

The viral genes were grouped into four clusters based on their expression patterns in infected cells (Fig. 2*H* and Dataset S2). The expression levels of viral genes in cluster 1 (57 genes) increased from 2 to 6 hpi and then remained relatively constant in subsequent stages. The expression levels of viral genes in clusters 2 and 3 (22 and 51 genes, respectively) were increased from 2 to 24 hpi. These three viral gene clusters included 33 of 43 transmembrane-associated genes (18, 19) (Dataset S2). The data indicated that transmembrane genes, including *E248R* and *E199L*, were expressed at low levels at 2 hpi and initiated the transcription process after 2 hpi, which might be involved in virus entry into host cells. Viral genes in cluster 4 (28 genes) were expressed at relatively high levels in early stages, slightly down-regulated at 15 hpi, and up-regulated thereafter. This cluster contained six of seven viral secretion-related genes. These results demonstrated the temporal dynamics and transcriptome phase of viral genes with distinct functions.

Interferon and Inflammatory Responses Are Activated in Macrophages Exposed to ASFV. We have shown that the transcriptomic pattern was changed in PAMs upon ASFV stimulation (Fig. 1*E* and *SI Appendix*, Fig. S1*I*). To further investigate the characteristics of macrophages under ASFV exposure, we generated a pseudobulk sample by calculating the average expression level of each gene in cells from a given time point. PCA revealed distinct differences in PC1 of pseudobulk samples generated from unexposed and exposed cells (*SI Appendix*, Fig. S4*A*). Genes which separated exposed samples from others were significantly up-regulated in exposed samples (two-tailed *t* test, $P = 4.9 \times 10^{-12}$), and Gene Ontology (GO) analysis revealed that these genes were enriched in "response in virus," "type I IFN signaling pathway," and "I-kappa B (κB) kinase/nuclear factor (NF)-κB signaling" (*SI Appendix*, Fig. S4*B* and Dataset S3). In contrast, genes which were significantly down-regulated in exposed samples (two-tailed *t* test, $P = 1.5 \times 10^{-6}$)
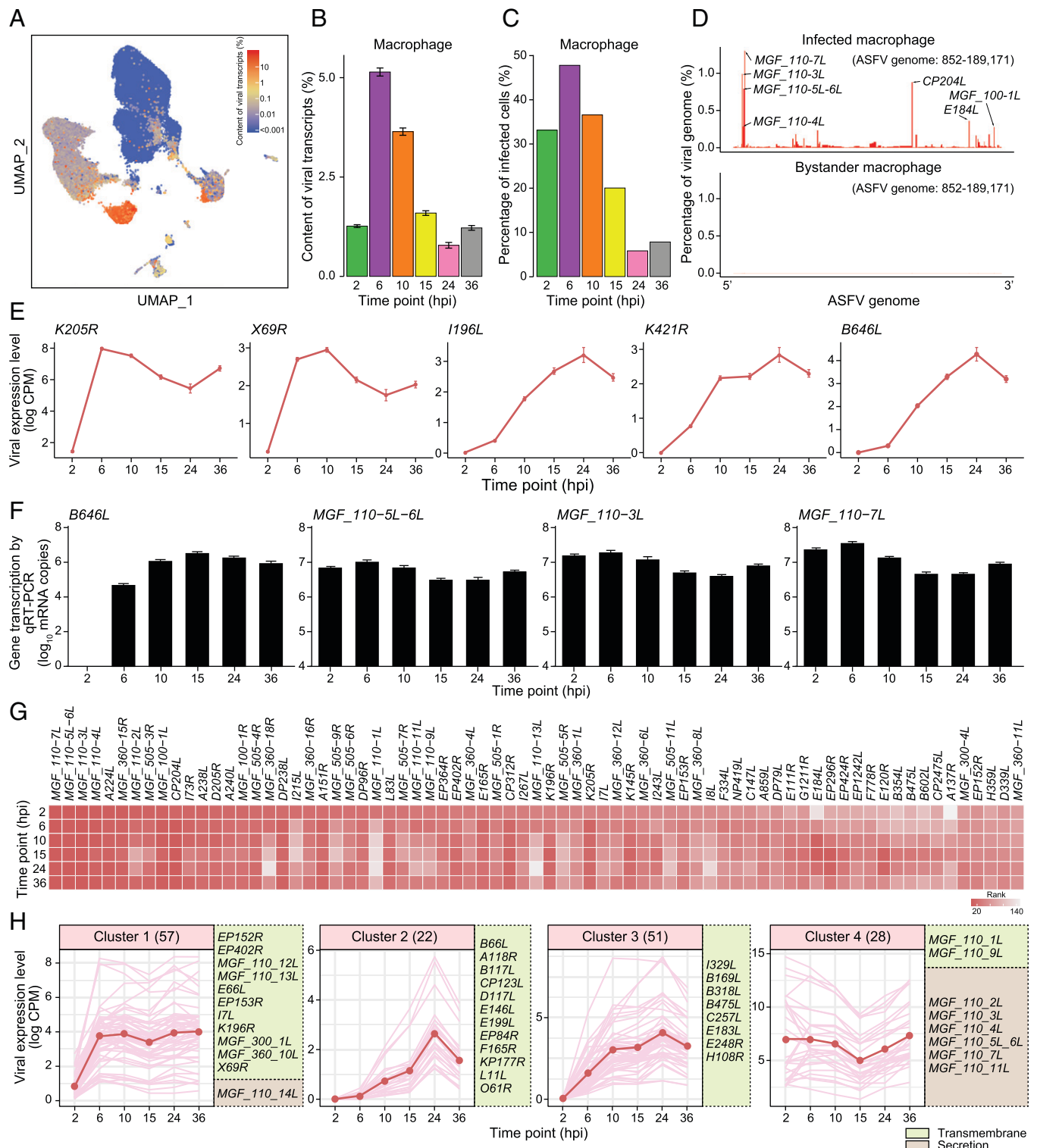
Fig. 2. Temporal dynamics of viral gene expression during ASFV infection. (*A*) UMAP plot showing the percentage of viral transcripts in each cell collected from all time points. (*B*) Bar plot showing the average percentage of the viral transcripts in macrophages. Data are shown as mean value ± SEM. (*C*) Bar plot showing the percentage of infected macrophages among living cells identified by scRNA-seq data. (*D*) Bar plots showing the percentage of transcripts for each viral gene in infected and bystander macrophages. (*E*) Line plots showing the expression levels of representative viral genes. Gene expression levels are quantified with counts per million mapped reads (CPM). Data are shown as mean value ± SEM. (*F*) Bar plots showing viral gene transcription by qRT-PCR. Data are shown as mean value ± SD. (*G*) Heatmap showing the rank of the top-ranked 50 viral genes in infected macrophages, ranked by the expressed frequency. (*H*) Line plots showing expression levels of viral genes in four gene clusters. The number of viral genes in each gene cluster is indicated in parentheses. Pink lines correspond to the expression levels of each gene, and red lines correspond to the average expression levels of genes. Transmembrane- and secretion-associated genes are indicated.

were associated with "positive regulation of apoptotic process" and "electron transport chain."

To understand the dynamic transcriptomic changes under ASFV exposure, we identified DEGs between unexposed and ASFV exposed cells. The majority of the 536 up-regulated and 838 down-regulated DEGs were commonly shared across multiple time points postinfection (Fig. 3*A* and Dataset S3). GO analysis results showed that genes involved in cytokine-mediated

signaling pathways, activation of the innate immune response, and regulation of type I IFN production were commonly up-regulated during infection (Fig. 3*B*). *TNFAIP3*, a core regulator of NF-κB activity induced by TNF-α (20), was also identified as an up-regulated DEG at all time points under ASFV exposure. Enzyme-linked immunosorbent assay (ELISA) and qRT-PCR results verified the up-regulation of TNF-α during infection (Fig. 3 *C* and *D*). Moreover, genes involved in the electron transport chain and metabolic process pathways were significantly down-regulated during infection.

IFN-stimulated genes (ISGs), including *ISG12*, *IFI6*, and *MX1*, were up-regulated in exposed cells. To assess the global ISG level and reflect the IFN response characteristics, we scored cells with expression levels of ISGs (Dataset S4). Compared with unexposed cells, we observed a significant up-regulation of ISG scores during infection at any time point (two-tailed *t* test, $P = 0$ for any time point), which suggested that the IFN signaling pathway was activated after cell exposure to ASFV (Fig. 3*E*). Inflammatory- and cytokine-related genes (for example, TNF-α and interleukin-1α [IL-1α]) were also increasingly expressed during infection (two-tailed *t* test, $P \leq 5.8 \times 10^{-84}$ for any time point) (Fig. 3*E* and Dataset S4). Notably, the median scores of ISGs gradually increased from 2 to 15 hpi, but inflammatory- and cytokine-related genes maintained high expression at the early stage of infection and gene scores had no obvious upward trend. These findings implied the asynchrony of gene activation related to various immune response pathways.

Transcriptional regulatory network analysis was applied to reveal potential core regulators using a modified version of the single-cell regulatory network inference and clustering (SCE-NIC) pipeline (21). Rather than using the entire gene expression data to perform SCENIC analysis, only up-regulated (or down-regulated) DEGs were loaded to prevent core regulators that were specifically expressed in exposed (or unexposed) cells from being overlooked. *STAT1* was identified as a potential key regulator among up-regulated DEGs at all time points, except 2 hpi, and ISGs including *IRF7* and *HIF1A* were implicated as having important roles in IFN response after macrophages are exposed (Fig. 3*F*). Core regulators and their target genes overlapped with many ISGs and inflammatory- and cytokine-related genes at 10 hpi, suggesting that functional genes involved in antiviral effects were up-regulated to defend against virus infection at this stage (Fig. 3*G*). Regulatory network visualization revealed that several genes were up-regulated by the core regulator *STAT1*, which is a core transcription factor in the Janus kinase/signal transducer and activator of transcription (JAK-STAT) pathway related to cytokine receptor signaling, and STAT1 stimulates inflammation and promotes cellular responses induced by IFN-γ (22) (Fig. 3*H*). The collective findings indicated the global effects on cells under ASFV exposure, and revealed the activated IFN and inflammatory responses during ASFV infection.

Up-Regulation of the Unfolded Protein Response in the Virus Early Replication Stage. Exposed cells could be grouped into bystander and infected cells. After elucidating the global alternation of gene expression profiles throughout ASFV, we next focused on molecular characteristics in infected cells. Compared with unexposed cells, DEGs and their enriched GO terms in infected cells were as similar as those in exposed cells (*SI Appendix*, Fig. S5 *A* and *B* and Dataset S3). Genes related to the response to TNF, IFN-γ, and NF-κB were up-regulated in infected cells, and down-regulated DEGs were associated with

processes utilizing the autophagy mechanism and localization within the membrane (*SI Appendix*, Fig. S5*B*). Widespread IFN-α/γ transcriptional response was detected in infected cells (two-tailed *t* test, $P \leq 3.3 \times 10^{-20}$ for any time point) (*SI Appendix*, Fig. S5*C*). These results suggested that the activation of host antiviral genes may antagonize viral replication.

Previous studies have revealed that the ER is essential for ASFV replication and maturation, and that ASFV infection in turn promotes ER stress, which is also known as the unfolded protein response (UPR) (23, 24). Accordingly, we examined the hallmark score of UPR, and found that scores were lower in cells with relatively high viral loads, and scores were anticorrelated with viral loads (Spearman correlation coefficient, ρ = −0.49; correlation test, $P = 7.4 \times 10^{-228}$) (Fig. 4*A*, *SI Appendix*, Fig. S5*D*, and Dataset S4). It is possible that numerous viral proteins are produced in the "viral factory" close to the nucleus, containing ER components, which results in the changes of UPR. We selected the highest and lowest top-ranked 10% of cells based on the viral load and analyzed UPR scores (Fig. 4*A* and *SI Appendix*, Fig. S5*E*). The UPR score was decreased in high viral load cells compared with unexposed cells at almost all time points, while it only increased in low viral load cells at 10 hpi (Fig. 4*B*). This result showed that ASFV may activate a part of the UPR pathway instead of all components. As previously reported, UPR is mediated by three transmembrane proteins: activating transcription factor 6 (ATF6), inositol-requiring enzyme 1 (IRE1), and protein kinase–like ER resident kinase (PERK) (25, 26) (Fig. 4*C* and Dataset S4). To further explore the UPR subpathway activated in infected cells, we investigated the expression levels of subpathway-related genes. Compared with unexposed cells, the PERK subpathway was clearly up-regulated in low viral load cells and was decreased in high viral load cells at multiple time points, but ATF6 and IRE1 subpathways were not activated during infection (Fig. 4*D*).

Taken together, these results revealed that the inflammatory pathway and IFN-α/γ were activated in infected cells, and suggested that the PERK-mediated UPR pathways were promoted in the ASFV early-replication stage but suppressed when virus copies increased. These findings provide insights for understanding of the mechanism of the host cell response during viral infection.

Transcriptomic Differences between Infected Macrophages with Distinct Viral Loads. Notably, the hallmark score of TNF-α signaling via NF-κB in infected cells had a bimodal distribution at any time point, except 2 hpi (*SI Appendix*, Fig. S6 *A* and *B*). For a given time point, we obtained infected cells located in peaks of the density distribution decay, and defined cell sets C1 and C2 corresponding to the lower and higher expression levels of hallmark scores, respectively. Viral loads in C1 were significantly higher than those in C2 (two-tailed *t* test, $P \leq 1.7 \times 10^{-17}$ for any time point, except 24 hpi), indicating that the distribution of hallmark scores was associated with viral loads in infected cells.

We subsampled cells of the highest and lowest top-ranked 10% of cells based on viral loads at each time point so that we could focus on molecular distinctions between cells in these two virus replication states (*SI Appendix*, Fig. S5*E*). DEGs between cells with high and low viral loads at the various time points showed distinct patterns. At 6 and 10 hpi, there were 1,523 and 1,456 DEGs, respectively, compared with 317 DEGs at 15 hpi, which ranked third (*SI Appendix*, Fig. S6 *C* and *D* and Dataset S5). Because most of the DEGs at 6 and 10
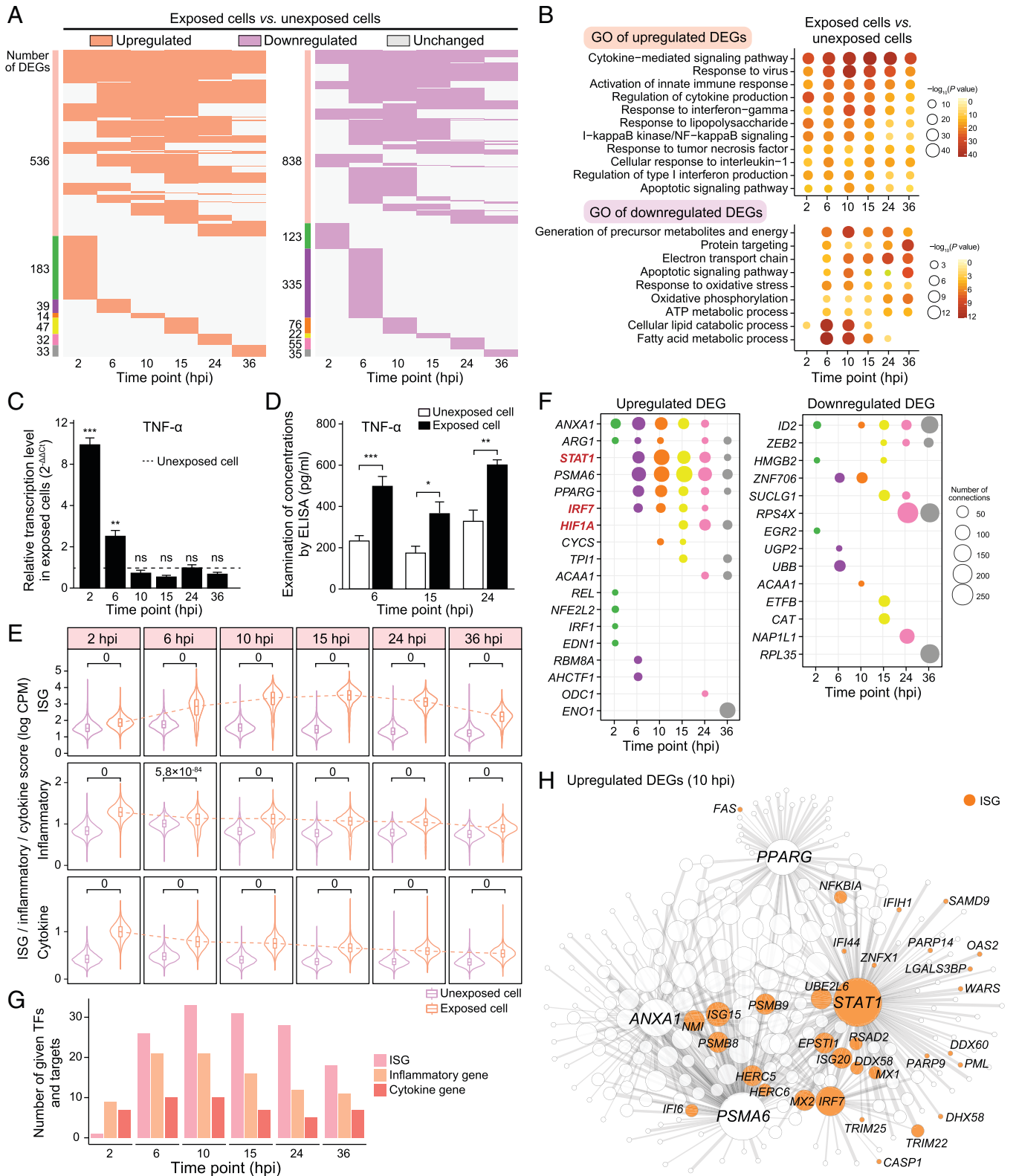
Fig. 3. Transcriptomic characteristics between unexposed and exposed cells. (*A*) Heatmaps showing the distribution of up-regulated and down-regulated DEGs between unexposed and exposed cells. The side bar indicates the DEG group (pink: DEGs shared by at least two time points; others: specifically expressed DEGs at one time point). (*B*) Dot plots showing enriched GO terms of up-regulated and down-regulated DEGs between unexposed and exposed cells. The dot color and size both indicate the statistical significance of the GO terms. (*C*) Bar plots showing the relative transcription level of TNF-α in exposed cells compared with unexposed. PAMs are examined by a relative qRT-PCR. ns, not significant; **$P < 0.01$ and ***$P < 0.001$ (two-tailed t test). Data are shown as mean value ± SD. (*D*) Bar plots showing the kinetics of TNF-α in the supernatants of unexposed and exposed cells. Supernatants are tested by ELISA. *$P < 0.05$, **$P < 0.01$, and ***$P < 0.001$ (two-tailed t test). Data are shown as mean value ± SD. (*E*) Violin and boxplots showing gene expression levels. Two-tailed t test P values are indicated. The dashed lines indicate the median trend of gene scores in exposed cells. (*F*) Dot plots showing potential key regulators in up-regulated and down-regulated DEGs during infection. The dot color and size indicate the time point and number of connections, respectively. ISGs are indicated in bold red. (*G*) Bar plot showing the number of overlapping genes between potential key transcription factors (TFs)/regulators/targets and given gene sets. (*H*) Gene regulation network showing potential key regulators and targets in up-regulated DEGs after infection at 10 hpi. The dot size indicates the number of connections, and the line thickness indicates the weight between a given gene pair.
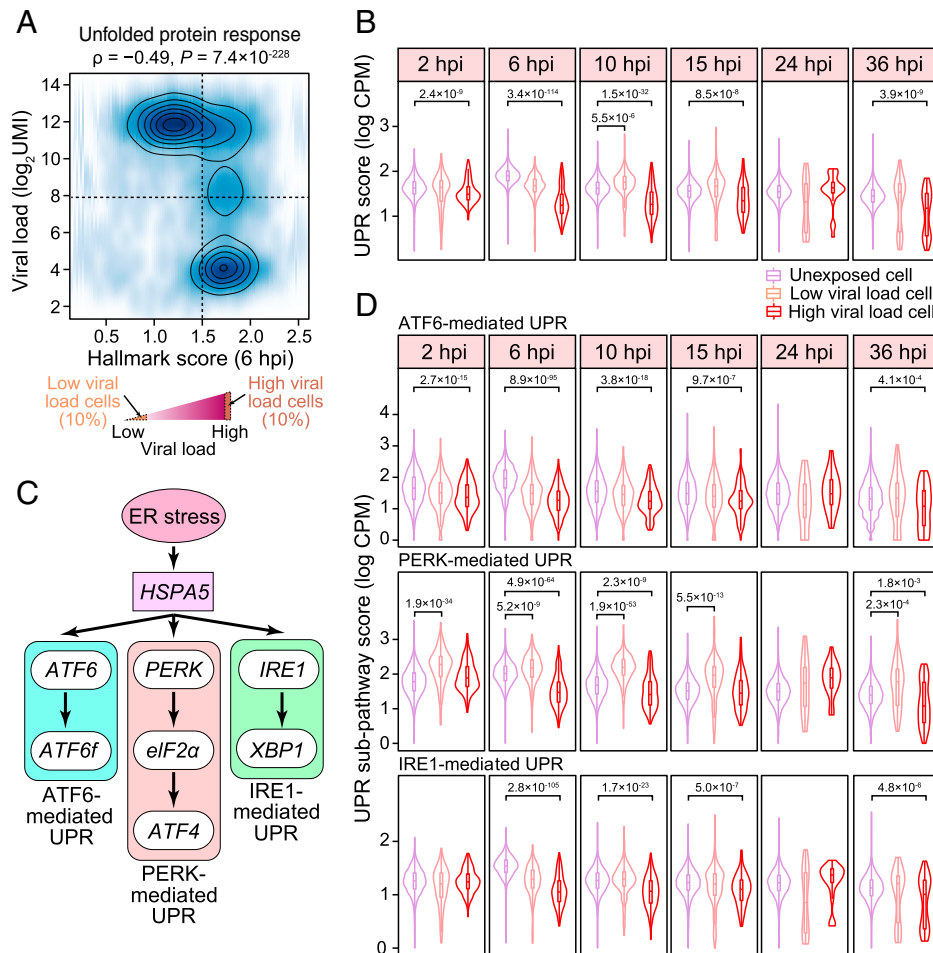
Fig. 4. Transcriptomic characteristics between unexposed cells and infected cells. (*A, Top*) Scatter density plots showing the relationship between viral loads and UPR hallmark scores in infected cells. Spearman correlation coefficients (ρ) and correlation test *P* values (*P*) are indicated. (*A, Bottom*) Schema showing the selection method of low and high viral load cells. (*B*) Violin and boxplots showing expression levels of UPR hallmark scores. Two-tailed *t* test *P* values are indicated. (*C*) Schema showing three UPR subpathways. (*D*) Violin and boxplots showing expression levels of UPR subpathway scores. Two-tailed *t* test *P* values are indicated.

hpi were shared with each other, we then analyzed DEGs at 6 hpi (Fig. 5*A* and *SI Appendix*, Fig. S6*C*). Mitochondrial genes, including *COX1* and *COX3*, and metabolic process–associated genes were up-regulated in high viral load cells (Fig. 5*A* and *SI Appendix*, Fig. S6*E*). Immune-related genes, including *CEBPB*, *BTG1*, *NEKBIA*, and several ISGs, were down-regulated in cells with high viral loads. The down-regulated DEGs were involved in "type I IFN production," "response to unfolded protein," and "Golgi vesicle transport" (Fig. 5*A* and *SI Appendix*, Fig. S6*E*).

Consistent with the UPR scores described above (Fig. 4*A*), inflammatory response scores ($\rho = -0.52$, $P = 8.2 \times 10^{-251}$) and ISG scores ($\rho = -0.48$, $P = 1.7 \times 10^{-216}$) were significantly negatively correlated with viral loads (*SI Appendix*, Fig. S6*F*). These results reflected viral entry-dependent changes in inflammatory and IFN pathways, and suggested that viral replication suppressed the expression of antiviral genes. Interestingly, when we examined hallmark/ISG scores along with the abundance of viral transcripts, a significant negative correlation (UPR, $\rho = -0.56$, $P = 6.8 \times 10^{-305}$; inflammatory response, $\rho = -0.57$, $P = 3.5 \times 10^{-315}$; ISG, $\rho = -0.57$, $P = 3.5 \times 10^{-317}$) was also detected (Fig. 5*B*). These results suggested that cells infected with various viral loads displayed signature transcriptomic changes at the median progression of infection (6 and 10 hpi).

Interactions between Host and Virus. To reveal the coregulated expression relationship between host and virus in infected cells, Spearman correlation analysis was performed for each viral gene and each host cellular gene. Instead of identifying DEGs between cells with high and low viral loads as described above, we tested the continuous relationship between viral and host gene expression levels. Viral genes involved in viral transcription (for example, *EP424R* and *H359L*) or the antagonism of the IFN pathway (for example, *MGF_360-21R* and *MGF_360-9L*) were highly correlated with the expression of host genes ($\rho \geq 0.3$, correlation test false discovery rate [FDR] ≤ 0.01, and percentage of expressed cells $\geq 10\%$) (Fig. 5*C*, *SI Appendix*, Fig. S7 *A–F*, and Dataset S5). Host genes whose expression levels were positively correlated with viral genes were related to translational initiation and the metabolism process (Fig. 5*C* and *SI Appendix*, Fig. S7 *A–E and G*). Consistent with the above results, IFN production and TNF-α signaling via NF-κB–associated genes were highly anticorrelated with virus genes. Notably, only two host genes were highly positively correlated with viral genes at 2 hpi, and *DUSP1* and *TMEM107* were especially correlated with 20 viral genes (*SI Appendix*, Fig. S7*A*). *TMEM107* encodes transmembrane protein 107, which is responsible for the development and regulation of cilia, and the lower expression of *TMEM107* was previously found to be associated with poorer prognosis in non–small-cell lung cancer
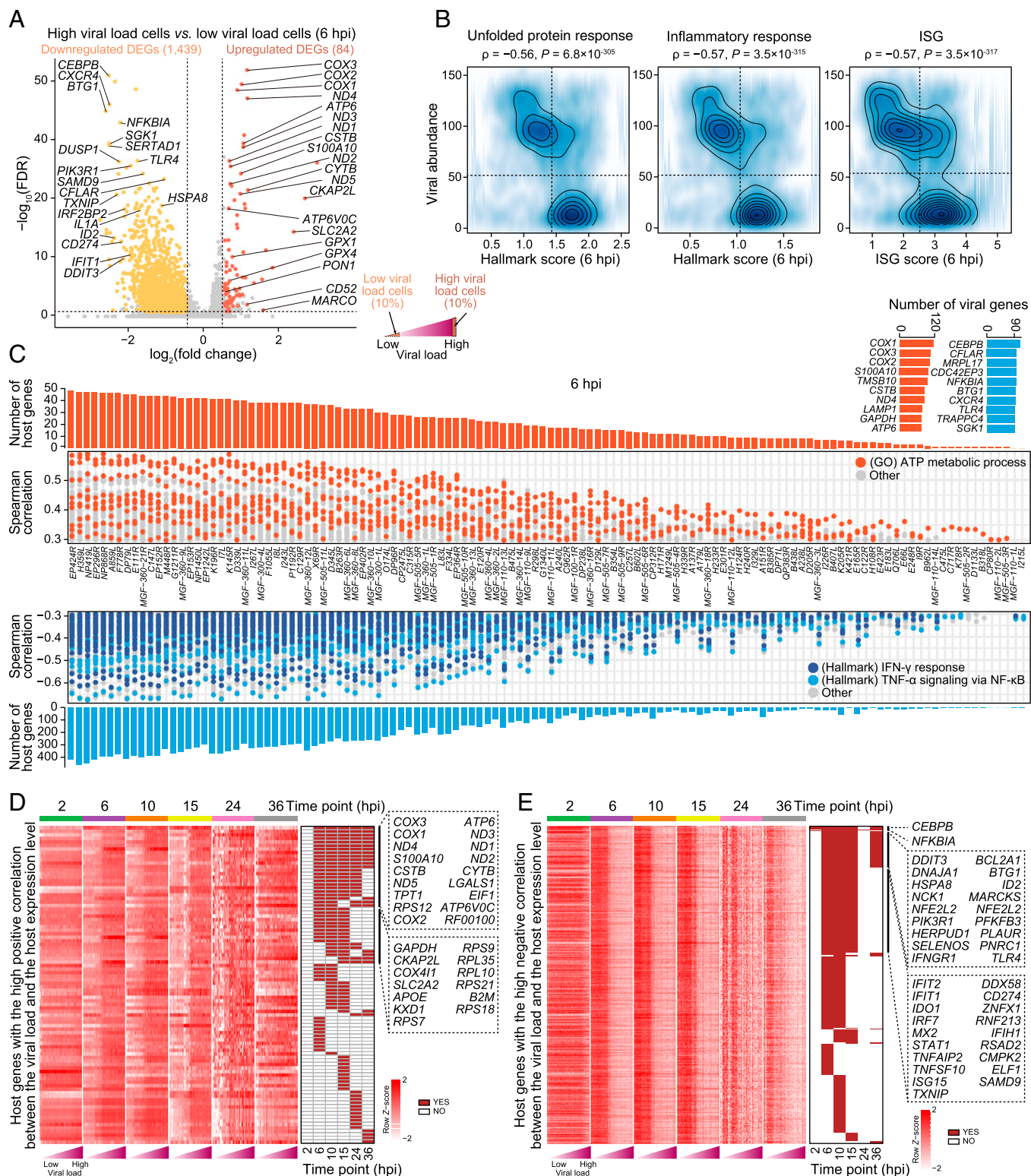
Fig. 5. Differences of host cells with distinct viral loads and coregulated analysis between host and virus. (*A*) Volcano plot showing DEGs between cells with high and low viral loads at 6 hpi. The numbers of up-regulated and down-regulated DEGs are indicated in parentheses. (*B*) Scatter density plots showing the relationship between viral abundance and hallmark/ISG scores in infected cells. Spearman correlation coefficients and correlation test *P* values are indicated. (*C*) Scatterplots showing the corresponding relationship between viral and host genes at 6 hpi. Each dot is a host gene, and host genes in given gene sets are colored. Bar plots (*Top* and *Bottom*) showing the number of host genes corresponding to a given viral gene and bar plots (*Top Right*) showing the number of viral genes corresponding to a given host gene and top-ranked 10 host genes are shown. (*D* and *E*, *Left*) Heatmap showing expression levels of host genes with a highly positive (*D*)/negative (*E*) correlation between viral loads and host expression levels, and cells are arranged into 100 bins and ordered with viral loads at each time point. (*D* and *E*, *Right*) Identification of genes corresponding to the heatmap (*Left*); red indicates that a given gene is the identified host gene with the high correlation at a given time point. Representative genes are listed.
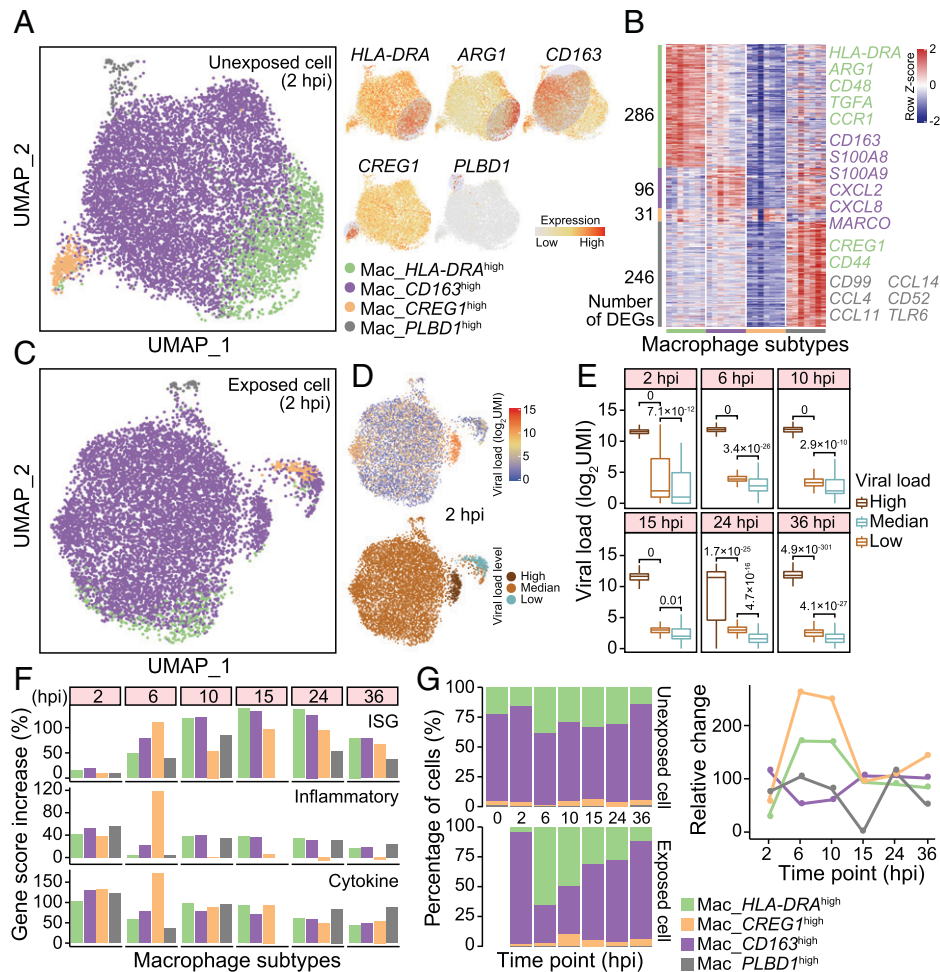
Fig. 6. Gene expression patterns of macrophage subtypes in the infection process. (*A*, *Left*) UMAP plot showing macrophage subtypes among unexposed cells at 2 hpi. (*A*, *Right*) UMAP plot showing expression levels of representative subtype-specific genes, and corresponding subtypes are indicated with shadows. (*B*) Heatmap showing scaled expression levels of macrophage subtype–specific genes. Each column corresponds to the average expression level of a given subtype at a given time point. Representative subtype-specific genes are listed (*Right*). (*C*) UMAP plot showing macrophage subtypes among exposed cells at 2 hpi. (*D*) UMAP plot showing viral loads and viral load levels of exposed cells at 2 hpi. Viral load levels are defined based on unsupervised clustering results. (*E*) Boxplots showing viral loads in cells with different viral load levels at each time point. Two-tailed *t* test *P* values are indicated. (*F*) Bar plots showing gene score increase in exposed cells, compared with unexposed cells. (*G*, *Left*) Stacked bar plot showing the percentage of macrophage subtypes among unexposed and exposed cells. (*G*, *Right*) Line plot showing the relative change of cell composition between unexposed and exposed cells.

(27, 28). Therefore, we inferred that viral infection triggered *TMEM107* expression to regulate cilia in the lung and further promote the infection process.

To identify host genes contributing to viral entry and defense, we explored the relationship between viral loads and host gene expression levels in infected cells. The expression levels of adenosine triphosphate (ATP) metabolic process– (for example, *COX1* and *ATP6*) and transcription- (for example, *RPS7* and *RPS9*) related genes were positively correlated with viral loads (Fig. 5*D*). ASFV induces mitochondrial aggregation around the "viral factory" in order to provide energy for virus production (29). Several ISGs (for example, *IFIT1* and *MX2*) and genes involved in virus defense were negatively correlated with viral loads, including *CEBPB*, at every time point, suggesting that antiviral genes continued to be suppressed with high viral loads in infected cells (Fig. 5*E*). The expression level of *STAT1*, a core transcriptional regulator of the IFN response, was decreased alongside viral replication. UPR-related genes, including *DDIT3* and *PIK3R1*, were negatively correlated with viral loads, indicating that increased viral replication suppressed the cell stress response. Thus, energy metabolic and immune function genes may be coregulated with viral infection.

Collectively, the data from differential expression analysis between cells with low and high viral loads and the host–virus interaction analysis both suggested that the up-regulation of metabolic pathways and the failed activation of the antiviral response are associated with viral replication within infected cells, and ASFV may evolve multiple strategies to shut off host IFN production and antiviral gene expression.

Roles of Macrophage Subtypes in ASFV Infection. We performed unsupervised clustering analysis for all unexposed macrophages and then separated them into four subtypes: Mac_*HLA-DRA*^high, Mac_*CD163*^high, Mac_*CREG1*^high, and Mac_*PLBD1*^high (Fig. 6 *A* and *B*, *SI Appendix,* Fig. S8 *A* and *B*, and Dataset S1). Mac_*HLA-DRA*^high highly expressed the major histocompatibility complex class II cell-surface receptor (encoded by *HLA-DRA*) and CC chemokine receptor 1 (encoded by *CCR1*). Mac_*CD163*^high highly expressed *CD163*, *MARCO*, *S100A8*, and *S100A9*. *MARCO* and *S100A8/9* were confirmed to play critical roles in the innate immune system during pathogenic infection (30). Therefore, we inferred that Mac_*CD163*^high is highly associated with the innate immune response. A previous study found that CD44 regulates macrophage recruitment to the lung in lipopolysaccharide-induced

airway disease (31), and we observed that Mac_CREG1^{high} expressed *CD44* and *CREG1*. Mac_PLBD1^{high}, which expresses *PLBD1*, is an interstitial macrophage in the lung and is associated with inflammation, and exists in interstitial spaces between alveoli (32). Various macrophage subtypes expressed different levels of immune-related genes, in which the expression levels of ISGs and inflammatory- and cytokine-related genes were low in Mac_CREG1^{high}, while Mac_PLBD1^{high} highly expressed these genes (*SI Appendix*, Fig. S9A). Subtype clustering results obtained from unexposed cells were mapped onto exposed cells, and macrophages were separated into four subtypes (Fig. 6C and *SI Appendix*, Fig. S8C). The distribution of single cells in UMAP plots followed viral loads instead of the subtype information (Fig. 6 D and E).

Although ISGs and inflammatory- and cytokine-related genes were up-regulated in exposed cells compared with unexposed cells (Fig. 3E), various macrophage subtypes showed different increased levels. Expression levels of ISGs were sharply raised in Mac_HLA-DRA^{high}, Mac_CD163^{high}, and Mac_CREG1^{high}, whereas Mac_PLBD1^{high} was slightly up-regulated (Fig. 6F). The most striking up-regulation of inflammation-related genes occurred in Mac_CREG1^{high} (1.2-fold increase) at 6 hpi, but there was essentially no change in the expression levels of these genes in Mac_CREG1^{high} at subsequent time points (Fig. 6F). We additionally investigated DEGs among distinct macrophage subtypes. The observed transcriptomic differences between exposed and unexposed macrophages were detected in Mac_HLA-DRA^{high} and Mac_CD163^{high}, which comprised 89.4 to 98.4% of macrophages at each time point (*SI Appendix*, Fig. S9B). We also performed GO analysis for these DEGs, and found that enriched GO terms of DEGs corresponding to Mac_HLA-DRA^{high} were as similar as these in Mac_CD163^{high} (*SI Appendix*, Fig. S9C and Dataset S6).

We then investigated the fraction change in macrophage subtypes among unexposed and exposed cells. The composition of macrophage subtypes dramatically changed during the progression of infection (Fig. 6G). At 2 hpi, Mac_CD163^{high} comprised 93.1 and 80.4% of cells among exposed and unexposed cells, respectively. However, the percentage dropped to 31.8% at 6 hpi and gradually increased thereafter among exposed cells. The percentages of Mac_HLA-DRA^{high} and Mac_CREG1^{high} are noteworthy, and the relative change of these two subtypes between unexposed and exposed cells increased from 2 to 6 hpi but decreased from 10 to 15 hpi.

Interestingly, the ratio of high viral load cells in each subtype remained roughly constant at 2 hpi, but 64.2 and 77.3% of Mac_CREG1^{high} were infected with high ASFV loads at 6 and 10 hpi, respectively (*SI Appendix*, Fig. S9D). As the infection progressed, the ratio of cells with high viral loads gradually decreased, and there were hardly any high viral load cells in Mac_HLA-DRA^{high} and Mac_CD163^{high} at 24 and 36 hpi. The above results suggested host cellular heterogeneity and susceptibility to ASFV infection, and implied that macrophage subtypes played distinct roles in ASFV invasion.

TNF-α Is Involved in the Cell Apoptosis Induced by ASFV Infection. ASFV infection induces cell death in macrophages, and apoptosis is one of the types of cell death (33). Apoptosis plays an important role in innate cellular responses to prevent viral infections (34). GO terms indicated that the genes involved in the apoptotic process were significantly altered during ASFV infection (Fig. 3B). Our scRNA-seq data revealed that 143 apoptosis signaling pathway–associated genes were differentially expressed at more than one time point, in which

70 and 73 genes were up-regulated and down-regulated, respectively (*SI Appendix*, Fig. S10). Furthermore, we demonstrated that ASFV infection induced higher-level apoptosis in exposed cells than that in unexposed cells using a fluorescence-activated cell sorting (FACS) method (Fig. 7 A and B). Thus, the dysregulation of the apoptosis-related pathway probably triggered the depletion of peripheral blood leukocytes following ASFV infection. We have shown that the production of TNF-α was increased upon ASFV infection (Fig. 3 C and D). It is well-accepted that TNF-α promotes cell apoptosis or cell survival by tightly regulated mechanisms, and TNF-α can trigger apoptosis through binding the TNF-α receptor to activate the extrinsic apoptosis pathway (35). Furthermore, TNF-α can promote cell survival via NF-κB signaling (36).

To investigate the effects of TNF-α induced by ASFV infection on cell apoptosis, an anti–TNF-α monoclonal antibody (MAb) was used to block the TNF-α signaling pathway. PAMs infected with ASFV (MOI 1) for 36 h in the presence of the anti–TNF-α MAb were used for analysis of cell apoptosis, and the isotype immunoglobulin G (IgG) was used as a negative control. We found that the ratios of cell apoptosis induced by ASFV infection were decreased from 46.1 to 33.3, 32.3, and 31.4% upon treatment with the anti–TNF-α MAb at various concentrations, indicating that TNF-α engages in the apoptosis induced by ASFV infection (Fig. 7 C and D).

Discussion

ASF is characterized by hemorrhage and high mortality, resulting in huge economic losses in the global pig industry. However, the underlying mechanisms of ASFV infection and pathogenicity remain unclear. scRNA-seq can identify cell subsets and evaluate the precise transcriptome phase of viral genes, which provides an opportunity to clarify the correlation between cellular heterogeneity and virus infection. In this study, with comprehensive transcriptome profiling of ASFV-infected PAMs, we revealed signaling pathways modulated by viral infection, and the majority of up-regulated genes in exposed cells were related to a chemokine-mediated signaling pathway and activation of innate immune response. More specifically, expression levels of antiviral genes were decreased with increased viral loads, indicating that viral genes inhibit host antiviral responses in infected cells.

Viral infections induce immune cells to produce cytokines and inflammatory factors. We demonstrated that NF-κB signaling involved in the production of cytokines was highly activated in exposed cells, as previously reported (37). The transcriptions of TNF-α, *TNFAIP2*, and *TNFAIP3* were up-regulated in our scRNA-seq data, indicating that the host inflammatory response was induced by virus stimulation. We have shown that the production of TNF-α is involved in cell apoptosis during ASFV infection, indicating that it is one mechanism of ASFV pathogenesis. Thus, a strategy targeting TNF-α could be a future target for antiviral drugs against ASFV infection.

Our results revealed that UPRs were enriched in low viral load cells. To facilitate viral growth, ASFV may reduce the response to ER stress by regulating host cellular translation or by modulating protein folding levels. A previous study has demonstrated that ASFV infection induces the up-regulation of the ER chaperones calnexin and calreticulin to enhance the ability of the ER to fold proteins (23). Furthermore, the ASFV genome encodes a variety of proteins that interfere with the host's innate immune system, inhibit and evade the host's
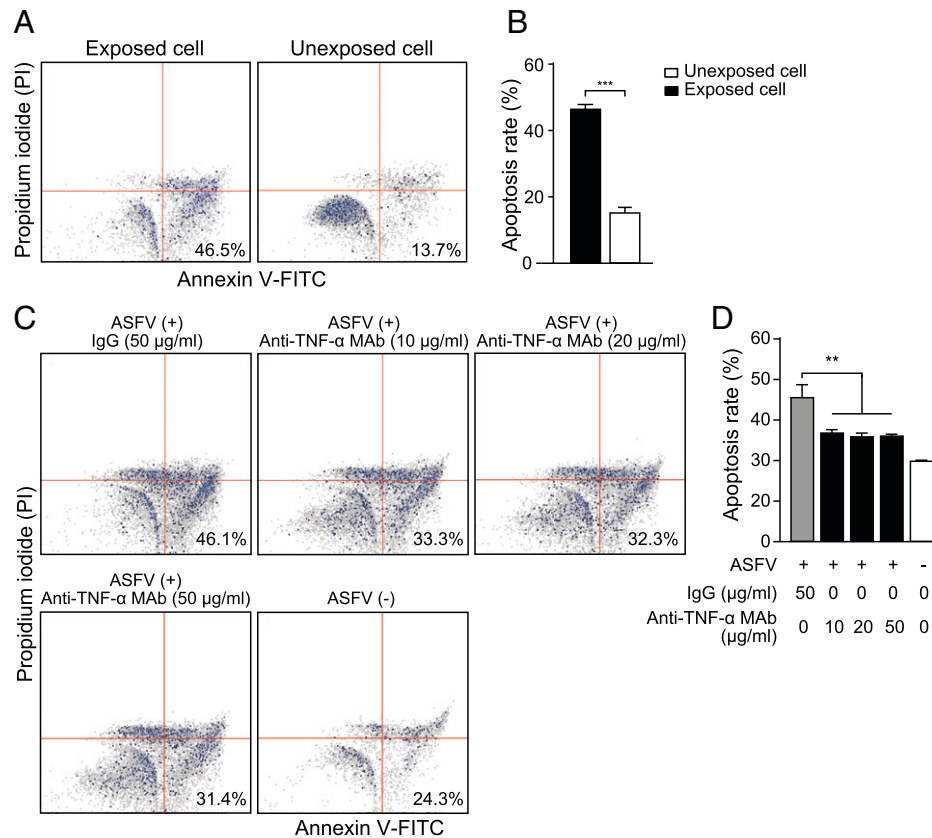
Fig. 7. TNF-α engages in cell apoptosis induced by ASFV infection. (*A* and *B*) FACS result showing cell apoptosis among unexposed or exposed cells. The apoptosis rate is shown in the scatter diagram (*A*) and quantified in the histogram (*B*). ***$P < 0.001$ (two-tailed *t* test). Data are shown as mean value ± SD. (*C* and *D*) FACS result showing cell apoptosis inhibited by an anti–TNF-α MAb. PAMs are exposed to ASFV at an MOI of 1 for 36 h in the presence of different concentrations (0, 10, 20, and 50 μg/mL) of anti–TNF-α MAb. The apoptosis rate in the cells is shown in the scatter diagram (*C*) and quantified in the histogram (*D*). **$P < 0.01$ (two-tailed *t* test). Data are shown as mean value ± SD.

immune response, and generate favorable conditions for virus growth (38, 39).

One interesting finding of this study is that some ASFV genes in the *MGF_110* family are commonly expressed at high levels during early and late infection. Considering their high levels of expression, it is likely that these genes play important roles throughout infection, which provides potential candidates for antiviral or vaccine targets. Furthermore, MGF_360 and MGF_530/505 can inhibit the production of type I IFN and the antiviral effect in the host, and the deletion of these genes in ASFV can induce the production of IFN in macrophages, thus attenuating virulence and providing protection against challenge with the parent virus in inoculated pigs (13, 14). Recently, the pMGF_505-7R protein has been proven to inhibit type I IFN and IL-1β by degrading STING with up-regulating *ULK1* expression, and the deletion of *MGF_505-7R* reduces virulence in pigs (40, 41).

We found up-regulation of the transcription-related enzymes and regulated factors of ASFV in the early or intermediate stages, indicating that ASFV is relatively less dependent on the host transcription machinery. We demonstrated that several members of the *MGF_110* family are highly transcriptional during the early stage of viral infection, as reported by a previous study (42). Additionally, mitochondria are recruited to the aforementioned virus factory to facilitate viral protein translation and virus assembly by providing energy for the virus life cycle. We observed that metabolic-related genes were down-regulated in exposed cells, suggesting that ASFV infection induces shutoff of host translation. In contrast, these genes were significantly up-regulated in infected cells with high viral loads,

indicating that these metabolic processes can be hijacked by ASFV for viral protein translation. ASFV DP71L can recruit protein phosphatase 1 to dephosphorylate eukaryotic initiation factor 2α (eIF2α) to restore protein synthesis and facilitate the production of viral proteins by hijacking the cellular protein translational machinery (43). ASFV pE66L inhibits host gene translation via the PKR/eIF2α pathway, and *E66L* gene deletion in ASFV causes a reduction in viral protein translation (44).

Two macrophage subtypes (M1 and M2) with different biological functions were identified in humans and mice. Since there were no previous studies on macrophage subtypes in pigs, we had attempted to annotate subtypes with well-known marker genes of M1 and M2. However, we found that the expression of these genes provided us less information to identify cell subtypes, probably due to species differences (*SI Appendix*, Fig. S8A). Therefore, we mainly analyzed host responses and virus–host interactions using the entire macrophage population to provide solid results, which was a limitation of this study. We will provide experiments to support biological functions of these macrophage subtypes and investigate their roles during ASFV infection in the future.

In summary, this work established a comprehensive viral and host dynamic transcriptome profile of ASFV-infected PAMs at single-cell resolution. We distinguished infected cells from all exposed cells in the ASFV-infected group, and transcriptome alternations of host cells were precisely determined in infected cells compared with those unexposed. Furthermore, we divided the infected cells into cells with high and low viral loads, and identified differences of host cells with distinct viral loads,

which are involved in ER stresses, inflammatory responses, and apoptosis. More specifically, we demonstrated that TNF-α production is necessary for cell apoptosis during ASFV infection. This study expands our understanding of ASFV–host interactions and the molecular events involved in viral replication and pathogenesis. Future studies need to focus on the important roles of signaling pathways or key molecules in the process of virus infection and pathogenicity, which may guide research on antiviral strategies.

Materials and Methods

Cells and virus, sample preparation for scRNA-seq, real-time RT-PCR, ELISA, annexin V/propidium iodide apoptosis assay, processing scRNA-seq data, identifying cell types and cell type–specific genes, identifying ASFV-infected cells, predicting virus contributions, clustering virus genes in infected cells, identifying DEGs between two groups, collection of different gene sets and calculation of gene scores, constructing transcriptional regulator networks, identifying host genes highly related to viral loads, calculating gene score increases in macrophage subtypes, calculating relative changes of macrophage subtypes, and statistical analysis are described in *SI Appendix, Materials and Methods*.

Data Availability. The raw and processed 10× Genomics data reported in this study have been deposited in the Gene Expression Omnibus under accession

number GSE168113 (45). All other study data are included in the article and/or supporting information.

Author affiliations: ªCAS Key Laboratory of Pathogen Microbiology and Immunology, Institute of Microbiology, Center for Influenza Research and Early-Warning (CASCIRE), Chinese Academy of Sciences (CAS), Beijing 100101, China; ᵇState Key Laboratory of Veterinary Biotechnology, National High-Containment Laboratory for Animal Diseases Control and Prevention, and National African Swine Fever Para-Reference Laboratory, Harbin Veterinary Research Institute, Chinese Academy of Agricultural Sciences, Harbin 150069, China; ᶜSavaid Medical School, University of the Chinese Academy of Sciences, Beijing 100049, China; ᵈBeijing Advanced Innovation Center for Genomics (ICG), Peking University, Beijing 100871, China; ᵉBiomedical Pioneering Innovation Center (BIOPIC), Ministry of Education Key Laboratory of Cell Proliferation and Differentiation, Peking University, Beijing 100871, China; and ᶠPeking-Tsinghua Center for Life Sciences (CLS), Academy for Advanced Interdisciplinary Studies, Peking University, Beijing 100871, China

1. C. L. Netherton, S. Connell, C. T. O. Benfield, L. K. Dixon, The genetics of life and death: Virus-host interactions underpinning resistance to African swine fever, a viral hemorrhagic disease. *Front. Genet.* **10**, 402 (2019).
2. L. Wang *et al.*, Comparative genomic analysis reveals an 'open' pan-genome of African swine fever virus. *Transbound. Emerg. Dis.* **67**, 1553–1562 (2020).
3. S. Liu *et al.*, Cryo-EM structure of the African swine fever virus. *Cell Host Microbe* **26**, 836–843.e3 (2019).
4. A. Malogolovkin, D. Kolbasov, Genetic and antigenic diversity of African swine fever virus. *Virus Res.* **271**, 197673 (2019).
5. G. Andrés, African swine fever virus gets undressed: New insights on the entry pathway. *J. Virol.* **91**, e01906-16 (2017).
6. E. R. Tulman, D. L. Rock, Novel virulence and host range genes of African swine fever virus. *Curr. Opin. Microbiol.* **4**, 456–461 (2001).
7. D. Kotliar *et al.*, Single-cell profiling of Ebola virus disease in vivo reveals viral and host dynamics. *Cell* **183**, 1383–1401.e19 (2020).
8. X. Ren *et al.*, COVID-19 immune features revealed by a large-scale single-cell transcriptome atlas. *Cell* **184**, 1895–1913.e19 (2021).
9. Y. Steuerman *et al.*, Dissection of influenza infection in vivo by single-cell RNA sequencing. *Cell Syst.* **6**, 679–691.e4 (2018).
10. P. G. Holt *et al.*, Extraction of immune and inflammatory cells from human lung parenchyma: Evaluation of an enzymatic digestion procedure. *Clin. Exp. Immunol.* **66**, 188–200 (1986).
11. H.-H. Takamatsu *et al.*, Cellular immunity in ASFV responses. *Virus Res.* **173**, 110–121 (2013).
12. I. Galindo *et al.*, African swine fever virus infects macrophages, the natural host cells, via clathrin- and cholesterol-dependent endocytosis. *Virus Res.* **200**, 45–55 (2015).
13. A. L. Reis *et al.*, Deletion of African swine fever virus interferon inhibitors from the genome of a virulent isolate reduces virulence in domestic pigs and induces a protective response. *Vaccine* **34**, 4698–4705 (2016).
14. L. Zsak *et al.*, African swine fever virus multigene family 360 and 530 genes are novel macrophage host range determinants. *J. Virol.* **75**, 3066–3076 (2001).
15. M. L. Nogal *et al.*, African swine fever virus IAP homologue inhibits caspase activation and promotes cell survival in mammalian cells. *J. Virol.* **75**, 2535–2543 (2001).
16. A. Brun, C. Rivas, M. Esteban, J. M. Escribano, C. Alonso, African swine fever virus gene A179L, a viral homologue of bcl-2, protects cells from programmed cell death. *Virology* **225**, 227–230 (1996).
17. A. Brun, F. Rodríguez, J. M. Escribano, C. Alonso, Functionality and cell anchorage dependence of the African swine fever virus gene A179L, a viral bcl-2 homolog, in insect cells. *J. Virol.* **72**, 10227–10233 (1998).
18. T. N. Petersen, S. Brunak, G. von Heijne, H. Nielsen, SignalP 4.0: Discriminating signal peptides from transmembrane regions. *Nat. Methods* **8**, 785–786 (2011).
19. A. Krogh, B. Larsson, G. von Heijne, E. L. L. Sonnhammer, Predicting transmembrane protein topology with a hidden Markov model: Application to complete genomes. *J. Mol. Biol.* **305**, 567–580 (2001).
20. I. Adrianto *et al.*; BIOLUPUS and GENLES Networks, Association of a functional variant downstream of TNFAIP3 with systemic lupus erythematosus. *Nat. Genet.* **43**, 253–258 (2011).
21. S. Aibar *et al.*, SCENIC: Single-cell regulatory network inference and clustering. *Nat. Methods* **14**, 1083–1086 (2017).
22. N. Au-Yeung, R. Mandhana, C. M. Horvath, Transcriptional regulation by STAT1 and STAT2 in the interferon JAK-STAT pathway. *JAK-STAT* **2**, e23931 (2013).
23. I. Galindo *et al.*, The ATF6 branch of unfolded protein response and apoptosis are activated to promote African swine fever virus infection. *Cell Death Dis.* **3**, e341 (2012).
24. I. Galindo, C. Alonso, African swine fever virus: A review. *Viruses* **9**, 103 (2017).
25. M. Schröder, R. J. Kaufman, The mammalian unfolded protein response. *Annu. Rev. Biochem.* **74**, 739–789 (2005).
26. J. Li *et al.*, A single-cell transcriptomic atlas of primate pancreatic islet aging. *Natl. Sci. Rev.* **8**, a127 (2020).
27. H. Xu *et al.*, TMEM107 inhibits EMT and invasion of NSCLC through regulating the Hedgehog pathway. *Thorac. Cancer* **12**, 79–89 (2021).
28. P. Cela *et al.*, Ciliopathy protein TMEM107 plays multiple roles in craniofacial development. *J. Dent. Res.* **97**, 108–117 (2018).
29. M. M. B. Moreno-Altamirano, S. E. Kolstoe, F. J. Sánchez-García, Virus control of cell metabolism for replication and evasion of host immune responses. *Front. Cell. Infect. Microbiol.* **9**, 95 (2019).
30. S. Wang *et al.*, S100A8/A9 in inflammation. *Front. Immunol.* **9**, 1298 (2018).
31. J. W. Hollingsworth *et al.*, CD44 regulates macrophage recruitment to the lung in lipopolysaccharide-induced airway disease. *Am. J. Respir. Cell Mol. Biol.* **37**, 248–253 (2007).
32. A. Kamei *et al.*, Exogenous remodeling of lung resident macrophages protects against infectious consequences of bone marrow-suppressive chemotherapy. *Proc. Natl. Acad. Sci. U.S.A.* **113**, E6153–E6161 (2016).
33. R. Portugal, A. Leitão, C. Martins, Apoptosis in porcine macrophages infected in vitro with African swine fever virus (ASFV) strains with different virulence. *Arch. Virol.* **154**, 1441–1450 (2009).
34. X. Zhou, W. Jiang, Z. Liu, S. Liu, X. Liang, Virus infection and death receptor-mediated apoptosis. *Viruses* **9**, 316 (2017).
35. F. H. Igney, P. H. Krammer, Death and anti-death: Tumour resistance to apoptosis. *Nat. Rev. Cancer* **2**, 277–288 (2002).
36. A. Hoffmann, D. Baltimore, Circuitry of nuclear factor kappaB signaling. *Immunol. Rev.* **210**, 171–186 (2006).
37. G. Cackett, R. Portugal, D. Matelska, L. Dixon, F. Werner, African swine fever virus and host response-transcriptome profiling of the Georgia 2007/1 strain and porcine macrophages. *J. Virol.* **96**, e0193921 (2022).
38. S. Correia, S. Ventura, R. M. Parkhouse, Identification and utility of innate immune system evasion mechanisms of ASFV. *Virus Res.* **173**, 87–100 (2013).
39. M. Frączyk *et al.*, Evolution of African swine fever virus genes related to evasion of host immune response. *Vet. Microbiol.* **193**, 133–144 (2016).
40. J. Li *et al.*, pMGF505-7R determines pathogenicity of African swine fever virus infection by inhibiting IL-1β and type I IFN production. *PLoS Pathog.* **17**, e1009733 (2021).
41. D. Li *et al.*, African swine fever virus MGF-505-7R negatively regulates cGAS–STING-mediated signaling pathway. *J. Immunol.* **206**, 1844–1857 (2021).
42. G. Cackett *et al.*, The African swine fever virus transcriptome. *J. Virol.* **94**, e00119-20 (2020).
43. F. Zhang, A. Moon, K. Childs, S. Goodbourn, L. K. Dixon, The African swine fever virus DP71L protein recruits the protein phosphatase 1 catalytic subunit to dephosphorylate eIF2α and inhibits CHOP induction but is dispensable for these activities during virus infection. *J. Virol.* **84**, 10681–10689 (2010).
44. Z. Shen *et al.*, A novel function of African swine fever virus pE66L in inhibition of host translation by the PKR/eIF2α pathway. *J. Virol.* **95**, e01872-20 (2020).
45. Y. Zheng *et al.*, Transcriptome profiling in swine macrophages infected with African swine fever virus at single-cell resolution. Gene Expression Omnibus. https://www.ncbi.nlm.nih.gov/geo/query/acc.cgi?acc=GSE168113. Deposited 5 April 2022.